J. Fluid Mech. (1985), *vol.* 153, *pp.* 1–16
Printed in Great Britain

Reflections from solitary waves in channels of decreasing depth

By C. J. KNICKERBOCKER
St Lawrence University, Department of Mathematics, Canton, NY 13617

AND ALAN C. NEWELL
Program in Applied Mathematics, University of Arizona, Tucson, AZ 85721

(Received 12 January 1981 and in revised form 26 January 1984)

We have found that the reflected wave that is created by a right-going solitary wave as it travels in a region of slowly changing depth does not satisfy Green's law. The amplitude of the reflected wave is constant along left-going characteristics rather than proportional to the negative fourth root of depth. This new finding allows us to satisfy the mass-flux conservation laws to leading order and establishes that the perturbed Korteweg–de Vries equation is a consistent approximation for the right-going profile.

1. Introduction

The changes that occur in a solitary wave as it propagates in a region of slowly varying depth (figure 1) have been the subject of many investigations beginning with Boussinesq in 1872. By applying the principle of conservation of energy, Boussinesq was able to describe the slow change in wave amplitude, but he also recognized that, even allowing for this modulation, the mass flux (also referred to as momentum; Miles 1979) was not conserved. Much later, the success of the Korteweg–de Vries (1895) equation as a model for describing the unidirectional propagation of long, low-amplitude surface waves, together with the development of sophisticated perturbation techniques, prompted renewed efforts on this problem beginning about ten years ago. Johnson (1973*a*) and Kakutani (1971) derived the appropriately perturbed Korteweg–de Vries equation; Johnson (1973*b*), Grimshaw (1970, 1971) and Leibovich & Randall (1973) made valuable and partially successful attempts to understand the slow changes which occur on the flow over long distances in which the depth changes by an order-one factor (the region $0 < \hat{x} < \hat{x}_f$ in figure 1). The difficulty they encountered was that the slowly changing solitary wave (its amplitude changes in inverse proportion to the local depth) cannot by itself satisfy the conservation of mass flux requirement of the perturbed Korteweg–de Vries equation. A secondary structure (Kaup & Newell 1978; Newell 1978; Karpman & Maslov 1977) is created, a shelf which extends between the solitary wave and that position to which infinitesimal disturbances would have travelled from the initial point at which the depth first begins to change. To leading order, the shelf may be treated by a linear model; it is a wave whose amplitude on creation (at the immediate rear of the solitary wave) may be calculated from the amount by which the slowly changing solitary wave fails to satisfy the local conservation of mass flux requirement for unidirectional flow; its subsequent evolution (Newell 1978; Miles 1979; Knickerbocker & Newell 1980) is described by Green's law; namely along a right-going characteristic the product of the shelf amplitude and the fourth root of the local depth is constant.

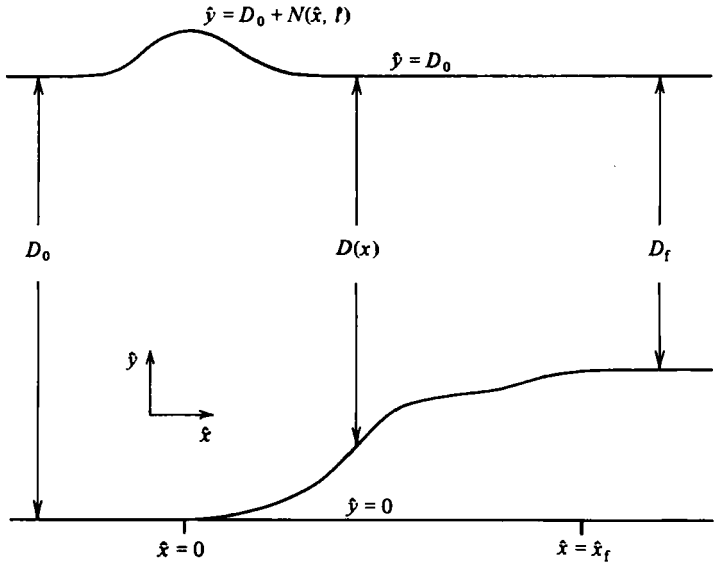

FIGURE 1. Physical system being considered, where $N(\hat{x}, \hat{t})$ is the dimensional elevation, $U(\hat{x}, \hat{t})$ is the dimensional horizontal velocity, $\hat{x}$ is space coordinate, $\hat{t}$ is time and $D(\hat{x})$ is the depth. For $\hat{x} < 0$, $D(\hat{x}) = D_0$, and for $\hat{x} > \hat{x}_f$, $D(\hat{x}) = D_f$.

However, the conservation of mass flux law for the perturbed Korteweg–de Vries equation ($\rho D_0^{\frac{1}{2}} \int_{-\infty}^{\infty} D^{\frac{1}{2}}(\hat{x})\, U(\hat{x}, \hat{t})\, \mathrm{d}\hat{t}$ is independent of $\hat{x}$; $\hat{t}$ is the time, $D(\hat{x})$ is the local depth, $U(\hat{x}, \hat{t})$ the horizontal velocity, ρ the density, g the acceleration due to gravity, and D_0 the constant local depth for $\hat{x} < 0$) is not the same as that for the full shallow-water-wave equations for which $\int_{-\infty}^{\infty} \rho D(\hat{x})\, U(\hat{x}, \hat{t})\, \mathrm{d}\hat{t}$ is independent of $\hat{x}$. This is because the changing depth causes a wave of reflection; although its amplitude is very small, over distances in which the depth changes by order one, the mass flux associated with it will be of the same order as that associated with the right-going component of the flow. The first attempt to calculate the reflected wave was made by Peregrine (1967), who computed the initial amplitude of the reflected wave, a result which is correct only for short times and distances. Recently the role of both the right- and left-going shelves was treated by Miles (1979). He used the same method by which the amplitude of the right-going shelf in the immediate rear at the solitary wave is calculated to calculate the amplitude at creation of the left-going disturbance; namely in the lee of the right-going disturbance (the solitary wave together with its trailing shelf), the amplitude of the left-going disturbance is computed (as we shall do in §2) from the amount by which the mass flux associated with the perturbed Korteweg–de Vries equation fails to satisfy the local conservation of mass flux for the full two-directional shallow-water-wave equations. Miles then used Green's law to describe the subsequent evolution of the left-going disturbance and found that the law of conservation of momentum for the two-directional flow remained unsatisfied. Miles then concluded that 'The...results suggest that solutions...such as that for a slowly varying solitary wave..., must be regarded with some caution.'

It is the purpose of this short note to correct this failure and to give the complete picture (in the sense that we describe all flow components which carry order-one mass flux) of what happens when a solitary wave

$$N(\hat{x}, \hat{t}) = \tfrac{4}{3}\eta_0^2 D_0 \epsilon\, \mathrm{sech}^2\, \eta_0 \left(-\hat{t}\left(\frac{\epsilon g}{D_0}\right)^{\frac{1}{2}} + \frac{\epsilon^{\frac{1}{2}}\hat{x}}{D_0} - \frac{2\eta_0^2 \epsilon^{\frac{1}{2}}\hat{x}}{3D_0} \right) \quad (\hat{x} < 0), \tag{1.1}$$

where $n(\hat{x},\hat{t}) = D^{\frac{1}{2}}U(\hat{x},\hat{t})/g^{\frac{1}{2}}$ is the surface elevation, propagates into a region where the depth changes slowly from one constant depth D_0 to another D_f (the local depth for $x > x_f$). The results are as follows.

(*a*) The solitary-wave horizontal velocity, amplitude and speed undergo a slow modulation; the first is inversely proportional to the depth to the three-halves power. That is,

$$U_s(\hat{x},\hat{t}) = \tfrac{4}{3}\eta_0^2 D_0^2 \epsilon g^{\frac{1}{2}} D^{-\frac{3}{2}} \operatorname{sech}^2(\eta_0 R) + O(\epsilon\sigma),$$

where

$$R = -\frac{\hat{t}(\epsilon g)^{\frac{1}{2}}}{D_0^{\frac{1}{2}}} + \frac{\epsilon^{\frac{1}{2}}\hat{x}}{D_0} - \frac{2\eta_0^2 \epsilon^{\frac{3}{2}}\hat{x}}{3D_0} \quad (\hat{x} < 0).$$

The solitary-wave component of the solution carries a mass flux of $\frac{8}{3}\eta_0 \rho \epsilon^{\frac{1}{2}} D_0 D$, where the small parameter $\epsilon^{\frac{1}{2}}\eta_0$ is found from the amplitude $\frac{4}{3}\eta_0^2 D_0 \epsilon$ of the incoming solitary wave (1.1).

(*b*) A right-going shelf which stretches from $\hat{\theta}_+ = 0$ (where

$$\hat{\theta}_+ = -t\left(\frac{g\epsilon}{D_0}\right)^{\frac{1}{2}} + \int_0^{x\epsilon^{\frac{1}{2}}/D_0} \left(\frac{D_0}{D(r)}\right)^{\frac{1}{2}} \mathrm{d}r$$

is the characteristic associated with the linearized equations and $\hat{\theta}_+ = 0$ begins at the point where depth begins to change) to the solitary wave will change according to Green's law. The horizontal velocity of the shelf is given by

$$U_+(\hat{x},\hat{t}) = \frac{-3}{\eta_0 (D_0\epsilon)^{\frac{1}{2}}} \frac{\mathrm{d}D}{\mathrm{d}\hat{x}} D^{-\frac{1}{4}}(\hat{x})\, D^{\frac{3}{4}}(\hat{\bar{x}}) + O(\epsilon\sigma^2),$$

where $\hat{\bar{x}}$ corresponds to the position of the solitary wave. The change in the depth with respect to the spatial variable $\hat{x}$ is of order $\epsilon^{\frac{3}{2}}\sigma$. The mass flux associated with the right-going shelf is $\frac{8}{3}\eta_0 \rho \epsilon^{\frac{1}{2}} D_0^{\frac{7}{4}} D^{\frac{1}{4}} - \frac{8}{3}\eta_0 \rho \epsilon^{\frac{1}{2}} D_0 D$. The connection between the solitary wave and the shelf can be established when one computes the correction to the amplitude and horizontal velocity of the solitary wave. When this calculation is performed one finds that the correction does not tend to zero in the lee of the solitary wave, but tends to $-3D^{\frac{3}{4}}D_{\hat{x}}/\eta_0(D_0\epsilon)^{\frac{1}{2}}$, a finite constant (Leibovich & Randall 1973). This constant is precisely the value that the shelf takes on when evaluated right behind the solitary wave (Knickerbocker 1984).

(*c*) A left-going shelf of reflection, which stretches from $\hat{\theta}_- = 0$, where

$$\hat{\theta}_- = \hat{t}\left(\frac{g\epsilon}{D_0}\right)^{\frac{1}{2}} + \int_0^{\hat{x}\epsilon^{\frac{1}{2}}/D_0} \left(\frac{D_0}{D(r)}\right)^{\frac{1}{2}} \mathrm{d}r$$

is the left-going characteristic associated with the linearized equations, to $\hat{\theta}_+ = 0$, is added to the solution in order to compensate for the mass flux discrepancy. It does not satisfy Green's law, but rather the amplitude, and equivalently the product of the local depth and the horizontal velocity, is constant along left-going characteristics. The horizontal velocity of the reflected wave is given by

$$U_-(\hat{x},\hat{t}) = \tfrac{1}{3}\eta_0 \epsilon^{\frac{1}{2}} D_0^{\frac{3}{4}} D_{\hat{x}} D^{-\frac{1}{4}}(\hat{\bar{x}}) D^{-1}(\hat{x}) + O(\epsilon^2\sigma^2),$$

where $(\hat{x},\hat{t})$ is a point in the region bounded by $\hat{\theta}_+ = 0$ and $\hat{\theta}_- = 0$. The mass flux associated with this component is $\frac{8}{3}\eta_0 \rho \epsilon^{\frac{1}{2}} D_0^{\frac{7}{4}} D_f^{\frac{1}{4}} - \frac{8}{3}\eta_0 \rho \epsilon^{\frac{1}{2}} D_0^{\frac{7}{4}} D^{\frac{1}{4}}$. This discontinuity along $\hat{\theta}_+ = 0$ between the left- and right-going flow is resolved by incorporating the third-derivative linear term, which becomes important in this region, into (2.8). The transition takes place in a distance of $\sigma^{-\frac{1}{3}}$ measured in the units of the solitary wave width and is given by the integral of the Airy function (Knickerbocker & Newell 1980).

The total mass flux, which is found by adding the mass flux due to each portion of the solution, is $\frac{8}{3}\eta_0\rho\epsilon^{\frac{1}{2}}D_0^{\frac{7}{2}}D_f^{\frac{1}{2}}$ and is equal to the flux of all right-going disturbances at the point after which no further depth changes and therefore no further reflection occurs. In particular, we note that as D_f becomes small the total mass flux approaches zero. In that case, practically all the water associated with the incoming wave is reflected and very little reaches the shore. All our results are confirmed by numerical experiments reported in §3.

2. Analysis

The shallow-water equations that describe the total flow (the propagation of a solitary wave and its trailing and reflected shelves) are, in non-dimensional coordinates,

$$n_t + (hu)_x = -\epsilon(un)_x + \frac{\epsilon}{6}h^3u_{xxx}, \tag{2.1}$$

$$u_t + n_x = -\epsilon uu_x + \frac{\epsilon}{2}h^2u_{xxt}. \tag{2.2}$$

The equations are respectively the kinematic boundary condition for the free surface and the horizontal momentum equation. In (2.1) and (2.2), $n(x,t)\,(=N/D_0)$, $u(x,t)\,(=U/\epsilon(gD_0)^{\frac{1}{2}})$, $x\,(=\hat{x}\epsilon^{\frac{1}{2}}/D_0)$ and $t\,(=\hat{t}(g\epsilon/D_0)^{\frac{1}{2}})$ are the non-dimensional elevation, horizontal velocity to leading order ($\bar{u} = u + \frac{1}{2}\epsilon h^2u_{xx}$, where $\bar{u}$ is the horizontal velocity at the surface), horizontal distance and time variables respectively. The non-dimensional depth $h(x) = D(\hat{x})/D_0$ changes from unity to D_f/D_0 in a distance $\hat{x}_f = O(1/\epsilon^{\frac{3}{2}}\sigma)$, where $0 < \epsilon \ll \sigma \ll 1$, which is long with respect to the width of the solitary wave and the length of the right-going shelf. The small parameter σ is related to the average slope of $D(\hat{x})$. Note that in dimensionless coordinates the amplitude of the solitary wave is order one, its width is order one; the amplitude of the right-going trailing shelf is order σ, its length is order $1/\sigma$ (figure 2); the amplitude of the reflected wave is order $\epsilon\sigma$ and its length is order $1/\epsilon\sigma$ (figure 3). To leading order in ϵ, the conservation law for the mass flux (the amount of water crossing a fixed station for all time) is, from (2.1),

$$\frac{\partial}{\partial x}\int_{-\infty}^{\infty} h(x)\,u(x,t)\,\mathrm{d}t = 0. \tag{2.3}$$

We may look for solutions n_+ and u_+ of (2.1) and (2.2) that depend on the right-going characteristic $\theta_+ = -t + \int_0^x \mathrm{d}r/[h(r)]^{\frac{1}{2}}$ and slowly on $X\,(=\epsilon x)$. In this situation, one finds that, to leading order,

$$n_+ = h^{\frac{1}{2}}u_+, \tag{2.4}$$

$$\left(\frac{\partial}{\partial t} + h^{\frac{1}{2}}\frac{\partial}{\partial x}\right)(h^{\frac{3}{4}}u_+) = \epsilon\left[-\tfrac{3}{2}h^{\frac{3}{4}}u_+\frac{\partial u_+}{\partial x} - \tfrac{1}{6}h^{\frac{13}{4}}\frac{\partial^3 u_+}{\partial x^3}\right] \tag{2.5}$$

and

$$\left(\frac{\partial}{\partial t} + h^{\frac{1}{2}}\frac{\partial}{\partial x}\right)(h^{\frac{1}{4}}n_+) = \epsilon\left[-\tfrac{3}{2}h^{-\frac{1}{4}}n_+\frac{\partial n_+}{\partial x} - \tfrac{1}{6}h^{\frac{11}{4}}\frac{\partial^3 n_+}{\partial x^3}\right]. \tag{2.6}$$

Note that the linear portions of (2.5) and (2.6) are Green's law; $h^{\frac{3}{4}}u_+$ and $h^{\frac{1}{4}}n_+$ are constants along the right-going characteristics $\theta_+ = -t + \int_0^x \mathrm{d}r/[h(r)]^{\frac{1}{2}}$. In terms of θ_+ and X, the transformation of $n_+(x,t)$ to $n(\theta_+, X)$ yields the perturbed Korteweg–de Vries equation

$$n_X + \tfrac{3}{2}h^{-\frac{3}{2}}nn_{\theta_+} + \tfrac{1}{6}h^{\frac{1}{2}}n_{\theta_+\theta_+\theta_+} = -\frac{1}{4}\left(\frac{h_X}{h}\right)n, \tag{2.7}$$

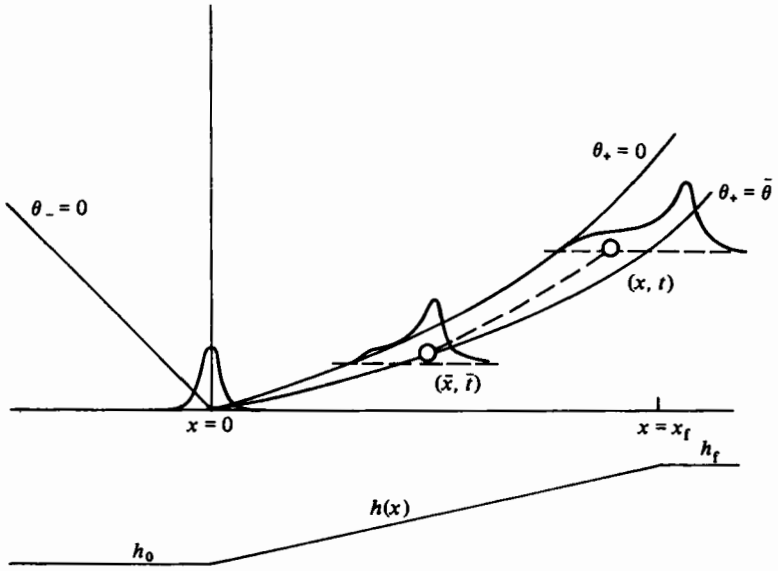

FIGURE 2. The evolution of a portion of the right-going shelf. The point $(\bar{x}, \bar{t})$ is the point of creation and the dashed line (– – – –) corresponds to the positive characteristic passing through $(\bar{x}, \bar{t})$ and (x, t).

and similarly for $u(\theta_+, X)$:

$$u_X + \tfrac{3}{2}h^{-1}uu_{\theta_+} + \tfrac{1}{6}h^{\frac{1}{2}}u_{\theta_+\theta_+\theta_+} = -\frac{3}{4}\left(\frac{h_X}{h}\right)u. \tag{2.8}$$

From (2.8) we find that

$$\frac{\partial}{\partial X}\int_{-\infty}^{\infty} h^{\frac{1}{2}}(X)\, u_+(\theta_+, X)\, \mathrm{d}\theta_+ = 0. \tag{2.9}$$

In order to solve (2.5) with the initial boundary conditions

$$n_+(0,t) = u_+(0,t) = \tfrac{4}{3}\eta_0^2 \operatorname{sech}^2(\eta_0 t) \quad (t \geqslant 0),$$
$$n_+(x,0)/h^{\frac{1}{2}} = u_+(x,0) = 0 \quad (x \geqslant 0),$$

we assume a solution of the form

$$n_+(x,t) = n_s(x,t) + \bar{n}_+(x,t), \quad u_+(x,t) = u_s(x,t) + \bar{u}_+(x,t), \tag{2.10}$$

where $n_s(x,t)$ and $u_s(x,t)$ are the amplitude and velocity of the solitary wave respectively, and $\bar{n}_+(x,t)$ and $\bar{u}_+(x,t)$ denote the amplitude and velocity of the right-going shelf respectively (note that the shelf is order σ in magnitude and non-zero only between $\theta_+ = 0$ and $\theta_+ = \bar{\theta}$, the position of the solitary wave (figure 2)).

To find the changes in the solitary wave $(n_s(x,t), u_s(x,t))$, we assume a leading-order solution of the form

$$u_s(x,t) = u_s(\theta_+, X) = A(X)\operatorname{sech}^2\{w(X)(\theta_+ - \bar{\theta})\}.$$

From (2.8) we find that

$$A(x) = \tfrac{4}{3}h^{\frac{1}{2}}w^2(X), \quad \bar{\theta}_X = \tfrac{2}{3}\eta_0^2 h^{-\frac{1}{2}}(X). \tag{2.11a}$$

From the conservation of energy,

$$\frac{\partial}{\partial X}\int_{-\infty}^{\infty} h^{\frac{3}{2}}(X)\,u^2(\theta_+, X)\,\mathrm{d}\theta_+ = 0,$$

we find that

$$\frac{\partial}{\partial X}\left(\frac{h^3 A^2}{w}\right) = 0. \tag{2.11b}$$

By combining (2.11*a*) and (2.11*b*), we find that $A(X) = \frac{4}{3}\eta_0^2 h^{-\frac{3}{2}}(x)$ and $w(x) = \eta_0 h^{-\frac{3}{2}}(X)$.

Therefore

$$u_s(x,t) = \tfrac{4}{3}\eta_0^2 h^{-\frac{3}{2}}\operatorname{sech}^2(\eta_0 h^{-\frac{3}{4}}(\theta_+ - \bar{\theta})), \tag{2.12a}$$

and from (2.4) the amplitude of the solitary wave is

$$n_s(x,t) = \tfrac{4}{3}\eta_0^2 h^{-1}\operatorname{sech}^2(\eta_0 h^{-\frac{3}{4}}(\theta_+ - \bar{\theta}))$$

The mass flux associated with the component is

$$m_s(x) = \tfrac{8}{3}\eta_0 h(x). \tag{2.12b}$$

Using (2.4) and approximating the x-derivatives on the right-hand side of (2.5) with t-derivatives, we find that

$$\frac{\partial}{\partial x}\int_{-\infty}^{\infty} h^{\frac{3}{2}}(x)\,u_+(x,t)\,\mathrm{d}t = 0. \tag{2.13}$$

Therefore, under the assumptions made in (2.10), we have

$$\frac{\partial}{\partial x}\int_{\bar{t}(x)}^{t_0(x)} h^{\frac{3}{2}}\bar{u}_+\,\mathrm{d}t = -\frac{\partial}{\partial x}\int_{-\infty}^{\infty} h^{\frac{3}{2}}u_s\,\mathrm{d}t, \tag{2.14}$$

where $t = \bar{t}(x)$ and $t = t_0(x)$ correspond to $\theta_+ = \bar{\theta}$ and $\theta_+ = 0$ respectively (figure 2). Since $\bar{u}_+(x,t)$ is assumed small and therefore changes according to the linear portion of (2.5), we have, upon differentiating the left-hand side of (2.14),

$$\bar{u}_+(\bar{x},\bar{t}) = \frac{-3h_x(\bar{x})\,h^{\frac{3}{2}}(\bar{x})}{\epsilon\eta_0},$$

where we have used the fact that $h^{\frac{3}{2}}\bar{u}_+$ is constant and where $(\bar{x},\bar{t})$ belongs to the path of the solitary wave (figure 2). From Green's law, which is valid because the change in $\bar{u}_+$ is fast with respect to the change in $h(x)$,

$$\bar{u}_+(x,t) = \frac{-3}{\epsilon\eta_0}h^{-\frac{3}{4}}(x)\,h^{\frac{3}{2}}(\bar{x})\,h_x(\bar{x}), \tag{2.15}$$

for any (x,t) lying between the solitary-wave path $\theta_+ = \bar{\theta}$ and $\theta_+ = 0$, and $(\bar{x},\bar{t})$ is the point at which the right-going characteristic through (x,t) meets $\theta_+ = \bar{\theta}$ (figure 2). The amplitude of the shelf can be found from (2.4), yielding

$$\bar{n}_+(x,t) = \frac{-3}{\epsilon\eta_0}h^{-\frac{1}{4}}(x)\,h^{\frac{3}{2}}(x)\,h_x(\bar{x}).$$

A little calculation (Knickerbocker & Newell 1979) shows that the mass flux $\bar{m}_+$ associated with the shelf component of the flow is

$$\bar{m}_+(x) = \int_{-\infty}^{\infty} h(x)\,\bar{u}_+(x,t)\,\mathrm{d}t = \tfrac{8}{3}\eta_0 h^{\frac{1}{2}}(x) - \tfrac{8}{3}\eta_0 h(x), \tag{2.16}$$

which, when added to the mass flux (2.12) associated with the solitary wave, gives $\frac{8}{3}\eta_0 h^{\frac{1}{2}}(x)$, which satisfies the equation for the right-going flux, but not (2.3), the total-mass-flux requirement.

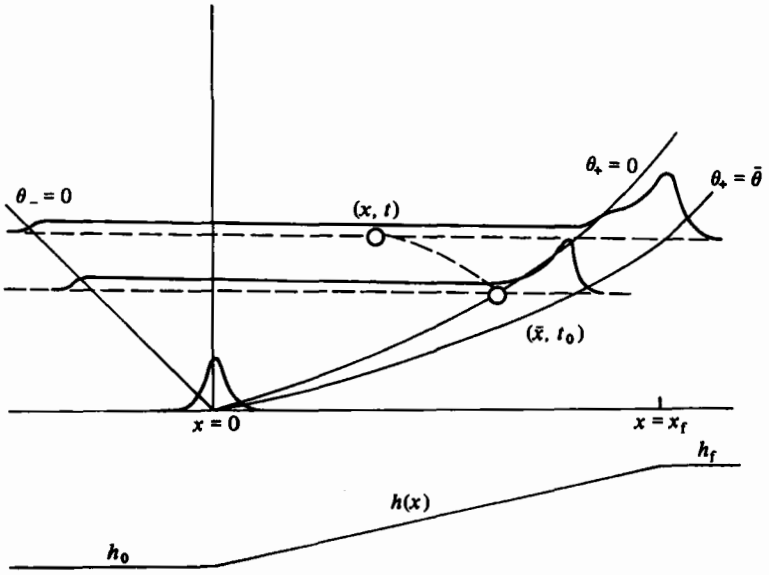

FIGURE 3. This figure shows the evolution of a portion of the left-going reflection. The point $(\bar{x}, t_0)$ is the point in space-time where the reflection measured at (x, t) is created. The negative characteristic $\theta_- = t + \int_0^x h^{-\frac{1}{4}}(r)\,dr$. The dashed line (– – – –) corresponds to the negative characteristic passing through $(\bar{x}, t_0)$ and (x, t).

In order to compensate for this discrepancy, it is necessary to add a left-going component $n_-(x,t)$ and $u_-(x,t)$ to the solution. Because of their very small amplitudes, $n_-(x,t)$ and $u_-(x,t)$ will satisfy the linearized versions of (2.1) and (2.2). The reflection will be non-zero in the region bounded by $\theta_- = 0$ and $\theta_+ = 0$ (figure 3). We first calculate their values along $\theta_+ = 0$ using the local conservation of mass flux. From (2.3) we have

$$\frac{\partial}{\partial x}\int_{-\infty}^{\infty} (h(x)\,u_+(x,t) + h(x)\,u_-(x,t))\,dt = 0.$$

Therefore

$$\begin{aligned}\frac{\partial}{\partial x}\int_{-\infty}^{\infty} h(x)\,u_-(x,t)\,dt &= -\frac{\partial}{\partial x}\int_{-\infty}^{\infty} h(x)\,u_+(x,t)\,dt \\ &= -\frac{\partial}{\partial x} h^{\frac{1}{4}}(x)\int_{-\infty}^{\infty} h^{\frac{3}{4}}(x)\,u_+(x,t)\,dt \\ &= -\tfrac{2}{3}\eta_0 h^{-\frac{3}{4}}(x)\,h_x(x) \quad (x < \bar{x}).\end{aligned}$$

When the solitary wave is at $(\bar{x}, t_0)$ (figure 3), the reflection contributed by the solitary wave up to that point will be non-zero from $t = t_0(x)$, which is the right-going characteristic $\theta_+ = 0$, and $t = t_-(x)$, which is the left-going characteristic initiated at $(\bar{x}, t_0)$. Therefore

$$\frac{\partial}{\partial x}\int_{-\infty}^{\infty} h(x)\,u_-(x,t)\,dt = \frac{\partial}{\partial x}\int_{t_0(x)}^{t_-(x)} h(x)\,u_-(x,t)\,dt$$

and

$$\frac{\partial}{\partial x}\int_{t_0(x)}^{t_-(x)} h(x)\,u_-(x,t)\,dt = -\tfrac{2}{3}\eta_0 h^{-\frac{3}{4}}(x)\,h_x(x) \quad (x < \bar{x}). \tag{2.17}$$

We differentiate the integral in (2.17), add and subtract $h(x)\,u_-(x,t_0)$ and use $(h(x)\,u_-(x,t))_x = -n_{-t}$ to find that

$$\begin{aligned} h(x)\,u_-(x,t_0) = {} & \tfrac{1}{3}\eta_0 h^{-\frac{1}{4}}(x)\,h_x(x) \\ & -\tfrac{1}{2}h^{\frac{1}{2}}[n_-(x,t_-)+h^{\frac{1}{2}}u_-(x,t_-)] \\ & +\tfrac{1}{2}h^{\frac{1}{2}}[n_-(x,t_0)+h^{\frac{1}{2}}u_-(x,t_0)]. \end{aligned} \tag{2.18}$$

In particular, (2.18) holds as x tends to $\bar{x}$, whence t_- tends to t_0. This is how Miles (1979) calculated $u_-(\bar{x},t_0)$. However, (2.18) yields two pieces of information. First,

$$u_-(\bar{x},t_0) = \tfrac{1}{3}\eta_0 h^{-\frac{5}{4}}(\bar{x})\,h_x(\bar{x}). \tag{2.19}$$

Secondly, we find that

$$(n_- + h^{\frac{1}{2}}u_-)|_{t_-} = (n_- + h^{\frac{1}{2}}u_-)|_{t_0}, \tag{2.20}$$

for any t_-, and therefore $n_- + h^{\frac{1}{2}}u_-$ is independent of time at any fixed x, that is

$$\frac{\partial}{\partial t}(n_- + h^{\frac{1}{2}}u_-) = 0. \tag{2.21}$$

In order to calculate $u_-(x,t)$ for points (x,t) (figure 3) in the region bounded by $\theta_- = 0$ and $\theta_+ = 0$, Miles applied Green's law to (2.19); that is, he took $h^{\frac{3}{4}}u_-$ constant along left-going characteristics. He also took $h^{\frac{1}{2}}n_-$ equal to $-h^{\frac{3}{4}}u_-$ to leading order. However, this leads to the total mass flux being $\frac{2}{3}\eta_0 h^{\frac{1}{2}}\ln(h_f/h) - \frac{8}{3}\eta_0 h^{\frac{1}{2}}$, which is clearly not constant. What is wrong?

It is incorrect to assume that Green's law holds for left-going disturbances. Green's law only holds when the depth $h(x)$ changes slowly with respect to the gradient of the disturbances in question. On the other hand, the reflected wave, by the very manner in which it is created, has a horizontal gradient that is of the same order as the gradient of the depth. However, (2.21),

$$n_{-t} + h^{\frac{1}{2}}u_{-t} = 0,$$

together with $n_{-t} + (hu_-)_x = 0$ gives us that

$$\left(\frac{\partial}{\partial t} - h^{\frac{1}{2}}\frac{\partial}{\partial x}\right)(hu_-) = 0 \tag{2.22a}$$

and

$$\left(\frac{\partial}{\partial t} - h^{\frac{1}{2}}\frac{\partial}{\partial x}\right)(n_-) = 0, \tag{2.22b}$$

which means that hu_- (and also n_-) is constant along left-going characteristics. Thus for a point (x,t) in the region bounded by $\theta_- = 0$ and $\theta_+ = 0$ the velocity of the reflected wave is

$$u_-(x,t) = \tfrac{1}{3}\eta_0 h_x(\bar{x})\,h^{-\frac{1}{4}}(\bar{x})\,h^{-1}(x). \tag{2.23}$$

The reflected mass flux measured along a constant x ($x = x_c$, figure 4), can be found by integrating the following expression:

$$\int_{-\infty}^{\infty} h(x_c)\,u_-(x_c,t)\,\mathrm{d}t. \tag{2.24}$$

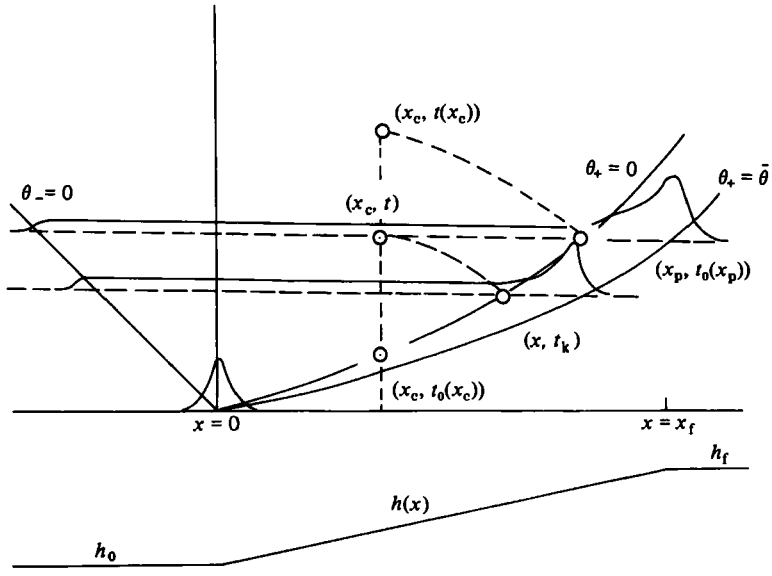

FIGURE 4. This figure shows the evolution of a portion of the left-going reflection. The point $(x_p, t_0(x_p))$ lies along $\theta_+ = 0$ and corresponds to the rear position of the right-going shelf. The line $x = x_c$ corresponds to the station at which the reflected mass flux is to be measured and $(x_c, t_0(x_c))$ and $(x_c, t_-(x_c))$. The point (x, t_k) is the intersection of the left-going characteristic through (x_c, t) and $\theta_+ = 0$.

But, as the right-going flow travels from $x = x_c$ to $x = x_p$, the reflected mass flux will be non-zero only between $(x_c, t_0(x_c))$ (which lies on the right-going characteristic $\theta_+ = 0$) and $(x_c, t_-(x_c))$ (which is the left-going characteristic initiated at $(x_p, t_0(x_p))$. Therefore,

$$\int_{-\infty}^{\infty} h(x_c)\, u_-(x_c, t)\, \mathrm{d}t = \int_{t_0(x_c)}^{t_-(x_c)} h(x_c)\, u_-(x_c, t)\, \mathrm{d}t.$$

We will convert this integration in t from $t_0(x_c)$ to $t_-(x_c)$ to an integration from $x = x_c$ to x_p along $\theta_+ = 0$. From (2.22a),

$$h(x_c)\, u_-(x_c, t) = h(x)\, u_-(x, t_k),$$

where (x, t_k) is the point of intersection of $\theta_+ = 0$ and the left-going characteristic propagating through (x_c, t).
This implies that

$$t_k + \int_0^x h^{-\frac{1}{2}}(r)\, \mathrm{d}r = t + \int_0^{x_c} h^{-\frac{1}{2}}(r)\, \mathrm{d}r,$$

or

$$t = t_k + \int_0^x h^{-\frac{1}{2}}(r)\, \mathrm{d}r - \int_0^{x_c} h^{-\frac{1}{2}}(r)\, \mathrm{d}r. \tag{2.25}$$

Also at the point (x, t_k), we have that

$$-t_k + \int_0^x h^{-\frac{1}{2}}(r)\, \mathrm{d}r = 0. \tag{2.26}$$

This gives us a relationship between t and x. From (2.25) and (2.26) we have

$$t = 2\int_0^x h^{-\frac{1}{2}}(r)\, \mathrm{d}r - \int_0^{x_c} h^{-\frac{1}{2}}(r)\, \mathrm{d}r,$$

or

$$\mathrm{d}t = 2h^{-\frac{1}{2}}(x)\,\mathrm{d}x. \tag{2.27}$$

Therefore the reflected mass flux is (figure 4)

$$\begin{aligned}\int_{-\infty}^{\infty} h(x_c)\,u_-(x_c,t)\,\mathrm{d}t &= \int_{t_0(x_c)}^{t_-(x_c)} h(x_c)\,u_-(x_c,t)\,\mathrm{d}t \\ &= \int_{t_0(x_c)}^{t_-(x_c)} h(x)\,u_-(x,t_k)\,\mathrm{d}t,\end{aligned}$$

or from (2.19) and (2.27)

$$\begin{aligned}&= \tfrac{2}{3}\eta_0 \int_{x_c}^{x_p} h^{-\frac{3}{4}}\,\mathrm{d}h \\ &= \tfrac{8}{3}\eta_0 h_1^{\frac{1}{4}}(x_p) - \tfrac{8}{3}\eta_0 h^{\frac{1}{4}}(x_c).\end{aligned}$$

Once the solitary wave has reached a constant depth ($x > x_f$) the mass flux associated with the reflected wave along any x is

$$m_-(x) = \int_{-\infty}^{\infty} h(x)\,u_-(x,t)\,\mathrm{d}t = \tfrac{8}{3}\eta_0 h_f^{\frac{1}{4}} - \tfrac{8}{3}\eta_0 h^{\frac{1}{4}}. \tag{2.28}$$

Adding this result to (2.12) and (2.16), the flux associated with the right-going component, we obtain for the total flux

$$\int_{-\infty}^{\infty} h(x)\,u(x,t)\,\mathrm{d}t = \tfrac{8}{3}\eta_0 h_f^{\frac{1}{4}}, \tag{2.29}$$

which is a constant and equal to the flux of the right-going component once the solitary wave has reached the point at which the depth again becomes constant.

In order to calculate the amplitude n_- of the reflected wave, we solve the linear Goursat problem defined as

$$\left.\begin{aligned} n_{-t} + (hu_-)_x &= 0, \\ u_{-t} + n_{-x} &= 0, \\ u_-(\theta_+ = 0) &= \tfrac{1}{3}\eta_0 h^{-\frac{5}{4}}(x)\frac{\mathrm{d}h}{\mathrm{d}x}(x). \\ u_-(\theta_- = 0) &= 0, \\ n_-(\theta_- = 0) &= 0. \end{aligned}\right\} \tag{2.30}$$

The reason that n_- is not equal to $-h^{\frac{1}{2}}u_-$ (in a manner analogous to $n_+ = h^{\frac{1}{2}}u_+$ for the right-going flow (2.4)) is that the premise by which the latter is derived neglects the smaller term $h_x u_+$. One cannot make this assumption for the reflected flow.

In §3 we show the results of solving the initial-value problem (2.1), (2.2) and the Goursat problem (2.30).

3. Numerical integration of the full shallow-water equations

In order to verify the results presented in §2, we simulated the full two-directional shallow-water equations (2.1) and (2.2) numerically. This simulation involved the use of a second-order-accurate finite-difference scheme with a variable spatial mesh.

Position x	Depth	Analytical $= \frac{8}{3}\eta_0 h^{\frac{1}{2}}(x)$	Numerical	Percentage error
25	0.976	3.05	2.99	1.97
101	0.901	2.99	2.92	2.34
202	0.803	2.90	2.84	2.07
308	0.693	2.80	2.73	2.50
372	0.637	2.74	2.66	2.92
432	0.578	2.67	2.58	3.37
490	0.521	2.61	2.51	3.83

TABLE 1. Comparison of the numerical right-going mass flux and the analytical right-going mass flux

All the numerical results presented here use $\epsilon = \frac{1}{64}$, $\sigma = \frac{1}{16}$, $\eta_0 = 1.15$, $h_0 = 1$, $h(x) = 1 - \epsilon\sigma x$, $h_f = \frac{1}{2}$, $x_f = 512$, $\Delta t = 0.075$ and

$$\Delta x_i = \Delta t\,[h(x_i)]^{\frac{1}{2}}\,(1 + \tfrac{2}{3}\epsilon\eta_0^2 h^{-2}(x_i)),$$

chosen so that $\Delta x_i/\Delta t$ is the speed of the solitary wave.

Since the analysis depends heavily on the mass-flux requirements, we first checked the right-going and total mass-flux laws at various stations between $x = 0$ and $x = x_f(h_f = \frac{1}{2})$. The results of the comparison of the numerical and analytical right going mass flux are given in table 1.

In table 2, we display the numerical results for the integrated mass flux

$$m(x, \theta_-) = \int_{-\infty}^{t_-} hu\,\mathrm{d}t, \quad t_- = \theta_- - \int_0^x \frac{\mathrm{d}x}{\sqrt{h}},$$

and the increment

$$\Delta m(x, \theta_-) = m(x, \theta_- - \Delta\theta_-) - m(x, \theta_-),$$

as function of θ_-, $0 < \theta_- < 1400$ for several stations x. The negative characteristic $\theta_- = 1200$ is the one which passes through the intersection of $\theta_+ = 0$ and $x = 512$, $h(512) = \frac{1}{2}$. This would be the last characteristic on which information is carried back if the transition along $\theta_+ = 0$ between right- and left-going flow components was sharp. In fact, the transition is described by an Airy function (Knickerbocker & Newell 1980) and occurs over a width of $\sigma^{-\frac{1}{3}}$ times the width of the solitary wave. Indeed we shall see in table 3 this is the width of the transition along $\theta_- = 1200$. Note that the data is consistent with our picture that the reflected wave generated along $\theta_+ = 0$ between $\theta_- - \Delta\theta_-$ and θ_- is carried back through this tube. In particular, both $m(x, \theta_-)$ and $\Delta m(x, \theta_-)$ are independent of x to within the order of approximation of (2.3) (approximately 3%). Moreover $m(x, \theta_-)$, $0 < \theta_- < 1200$ is precisely the total right-going flux at the station at which the curve $t + \int_0^x (\mathrm{d}x/\sqrt{h}) = \theta_-$ meets $\theta_+ = 0$ and would be the total mass flux if the depth were to become constant after this point. We emphasize that the reflection is generated all along $\theta_+ = 0$. In order to make sure that the discontinuities in $h(x)$ at $x = 0$ and $x = 512$ play no significant role, we repeated the calculation with a cubic shaped bottom.

Table 3 displays the incremental mass flux $\Delta m(x, t) = m(x, t) - m(x, t - 1.5)$ for

x...	−9.9	24.8	101.3	202.1	308.4	371.4	432.0	487.6	547.5
$h(x)$ ...	1.00	0.98	0.90	0.80	0.70	0.64	0.58	0.52	0.5
θ_-									
1400	2.55	2.55	2.53	2.52	2.50	2.49	2.49	2.48	2.48
	0.00	0.00	0.01	0.01	0.00	0.00	0.00	0.00	
1300	2.55	2.55	2.53	2.51	2.50	2.49	2.49	2.48	
	0.00	0.00	0.00	0.00	0.00	0.01	0.00	0.01	
1200	2.55	2.55	2.53	2.51	2.50	2.50	2.49	2.49	
	0.04	0.04	0.04	0.05	0.05	0.05	0.05		
1100	2.60	2.59	2.58	2.56	2.55	2.55	2.54		
	0.04	0.04	0.04	0.05	0.05	0.04			
1000	2.64	2.63	2.62	2.61	2.60	2.59			
	0.04	0.05	0.05	0.04	0.04	0.05			
900	2.68	2.68	2.67	2.65	2.64	2.64			
	0.04	0.04	0.04	0.05	0.05				
800	2.72	2.72	2.71	2.70	2.69				
	0.04	0.04	0.04	0.04	0.04				
700	2.76	2.76	2.75	2.74	2.73				
	0.04	0.04	0.04						
600	2.80	2.80	2.79						
	0.04	0.03							
500	2.84	2.83							
	0.04	0.04							
400	2.88	2.87							

TABLE 2. This table gives the mass flux and change in the mass flux at various positions in the x, θ_- plane. Within each entry of the table the top number is the total mass flux measured along a constant x from $t = -\infty$ up to that left-going characteristic $\theta_- = t + \int_0^x h^{-\frac{1}{2}}(r)\,dr$. The bottom number is the mass flux measured between two consecutive left-going characteristics listed on the table.

$x = 371.5$. Note the solitary wave, the right-going shelf, the oscillatory tail, the long reflection and the sharp drop at the *last* negative characteristic $\theta_- = 1200$. Table 4 is a comparison at several stations x of the times $t = 1200 - \int_0^x (dx/\sqrt{h})$ and the times in the numerical experiment at which the increment in the reflected mass flux decreased by a factor of 2.

We also checked various components of the analytical solution against the numerical results. First, we compared the maximum horizontal velocity of the analytical solitary wave ($\max(u_s(x,t)) = \frac{4}{3}\eta_0 h^{-\frac{3}{2}}(x)$) against the maximum horizontal velocity of the numerical solitary wave. The results of this comparison can be found in table 5.

A graphical representation of the comparison between the numerical and analytical solitary waves at $t = 500$ can be found in figure 5. We also checked the analytical predictions of the horizontal velocity for the right shelf against the numerical experiment. The results of this comparison can also be seen in figure 5. Except for a slight phase shift (less than 5%), it can be seen that the analytical predictions and the numerical results for the right-going flow are very close.

The numerical evidence supports our theoretical picture which asserts that the right-going flow component is described by the perturbed Korteweg–de Vries equation (2.8) and the left-going flow component is found by solving the Goursat problem (2.30). While Table 2 showed clearly that the incremental mass flux carried through the tubes $(\theta_- - \Delta\theta_-, \theta_-)$ is constant in x, we would like to verify (2.22) along

Time	Mass flux	Change in mass flux
	Solitary wave	
423.0	0.04	-0.04
424.5	1.78	-1.74
426.0	1.98	-0.20
427.5	2.09	-0.11
	Right-going shelf	
429.0	2.22	-0.13
430.5	2.37	-0.15
432.0	2.52	-0.15
433.5	2.63	-0.05
435.0	2.68	-0.05
	Oscillatory tail	
436.5	2.67	0.39×10^{-2}
444.0	2.66	-0.18×10^{-2}
451.5	2.65	0.85×10^{-3}
459.0	2.65	0.11×10^{-2}
	Left-going reflection	
465	2.65	0.91×10^{-3}
570	2.60	0.69×10^{-3}
666	2.56	0.70×10^{-3}
787.5	2.50	0.73×10^{-3}
	No further reflection	
796.5	2.49	0.26×10^{-3}
851.0	2.49	0.20×10^{-4}
948	2.49	0.40×10^{-5}

TABLE 3. Table 3 presents the mass flux and the change in the mass flux measured along a constant x ($x = 371.5$) at various times. The first column gives the time units (note the difference in the timescales between the various sections), the second column represents the total mass flux measured at $x = 371.5$ up to the given time and column 3 gives the mass flux measured only over the previous 1.5 time units.

x	$h(x)$	Analytic time	Numerical time
24.8	0.98	1175	1180
101.3	0.90	1096	1101
202.1	0.80	987	991
308.4	0.70	864	867
371.4	0.64	787	791
432.0	0.58	709	714
487.6	0.52	634	633

TABLE 4. Comparison at various depths of the analytical and numerical times at which no further reflection is measured. The analytical time is calculated from $t = 1200 - \int_0^x h^{-\frac{1}{2}}(r)\,dr$, while the numerical time is given as the time at which the change in the mass flux decreases by a factor of 2.

Numerical position	Depth	Analytical $\frac{4}{3}\eta_0^2 h^{-\frac{1}{2}}(x)$	Numerical	Percentage error
10.4	0.99	1.79	1.76	1.5
99.3	0.90	2.05	1.96	4.4
211.9	0.79	2.50	2.37	4.9
317.8	0.69	3.08	2.93	5.0
417.6	0.59	3.86	3.69	4.4
509.7	0.50	4.95	4.76	4.0

Table 5. Comparison of the maximum analytical horizontal velocity and the maximum numerical horizontal velocity at various positions

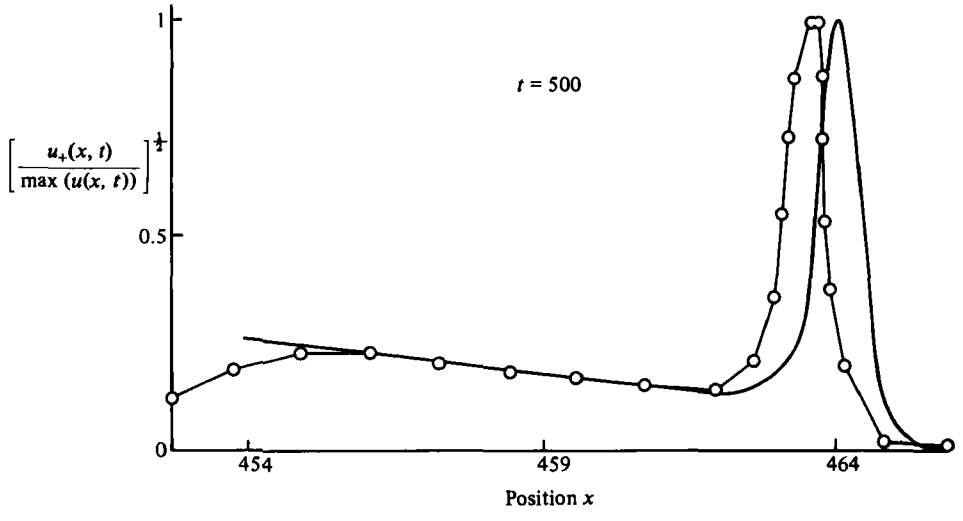

FIGURE 5. This figure shows the comparison between the numerical right-going flow (–○–) and the analytical right-going flow (——) versus the spatial coordinate x at time $t = 500$. Both curves were scaled by taking the square root of the normalized value.

each negative characteristic individually. This is not possible to do using the results of the first numerical scheme because even though the mass flux data is accurate, the pointwise date is not sufficiently good. Accordingly, we solved the Goursat problem defined by (2.30) numerically and found:

(1) $n_- + h^{\frac{1}{2}}u_-$ is independent of time along a constant x (2.31):

(2) hu_- and n_- ((2.22a, b) respectively) are constants along left-going characteristics;

(3) the reflected mass flux is given by (2.28).

We first checked the mass flux $\int_{-\infty}^{\infty} hu_- \, dt$ given by the numerical experiment against (2.28) and found close agreement. The relative error was much less than 1 % for all cases.

We next checked the constancy of $n_- + h^{\frac{1}{2}}u_-$ along a constant x. Because n_- and $h^{\frac{1}{2}}u_-$ are of the order of $\epsilon\sigma$ and their individual time derivatives are of the order of $\epsilon^2\sigma^2$, we must show that the time derivative of the sum is small with respect to $\epsilon^2\sigma^2$. The numerical experiments showed that the average of the gradient of $n_- + h^{\frac{1}{2}}u_-$ was of the order of $\epsilon^3\sigma^3$. These results are shown in table 6.

x	$h(x)$	$\epsilon\sigma$	$(\epsilon\sigma)^3$	$\frac{\partial}{\partial t}(n_- + h^{\frac{1}{2}}u_-)$
25.6	0.95	$\frac{1}{512}$	7.5×10^{-9}	6.4×10^{-9}
25.6	0.90	$\frac{2}{512}$	6.0×10^{-8}	5.1×10^{-8}
25.6	0.80	$\frac{4}{512}$	4.8×10^{-7}	4.0×10^{-7}
25.6	0.70	$\frac{6}{512}$	1.6×10^{-6}	1.8×10^{-6}
25.6	0.65	$\frac{7}{512}$	2.6×10^{-6}	6.2×10^{-6}

TABLE 6. A comparison of $\partial(n_- + h^{\frac{1}{2}}u_-)/\partial t$ and $(\epsilon\sigma)^3$ for various $\epsilon\sigma$

$\epsilon\sigma$	$\epsilon^3\sigma^3$	$\left(\frac{\partial}{\partial t}+h^{\frac{1}{2}}\frac{\partial}{\partial x}\right)(hu_-)$	$\left(\frac{\partial}{\partial t}+h^{\frac{1}{2}}\frac{\partial}{\partial x}\right)n_-$
$\frac{1}{128}$	4.8×10^{-7}	2.1×10^{-7}	2.3×10^{-7}
$\frac{1}{256}$	6.0×10^{-8}	2.4×10^{-8}	2.4×10^{-8}
$\frac{1}{512}$	7.5×10^{-9}	4.6×10^{-9}	4.3×10^{-9}
$\frac{1}{1024}$	9.3×10^{-10}	8.0×10^{-10}	7.6×10^{-10}

TABLE 7. A comparison of the changes in hu_- and n_- with $(\epsilon\sigma)^3$ for various slopes $\epsilon\sigma$ along $\theta_- = 101$

We also checked hu_- and n_- along negative characteristics ((2.22a, b) respectively) and found that the changes in hu_- and n_- along negative characteristics were of the order of $\epsilon^3\sigma^3$. Table 7 contains the results from various cases checked along a typical θ_- characteristic.

Note added in proof. If, in table 2, we had used the exact conservation law given by (2.2), we would find that

$$\int_{-\infty}^{\infty}(n+\tfrac{1}{2}\epsilon u^2)\,\mathrm{d}t$$

is independent of x to an accuracy of less than 1 %.

REFERENCES

BOUSSINESQ, J. 1872 Theorie des ondes des remous qui se propagert le long d'un rectangulaire horizontal, en communiquant au liquide contenu dans ce canal des sensiblement pareilles de la surface au fond. *J. Math. Pures Appl.* **17**, 55–108.

GRIMSHAW, R. 1970 The solitary wave in water of variable depth. *J. Fluid Mech.* **42**, 639–656.

GRIMSHAW, R. 1971 The solitary wave in water of variable depth. Part 2. *J. Fluid Mech.* **46**, 611–622.

JOHNSON, R. S. 1973*a* Asymptotic solution of the Korteweg–de Vries equation with slowly varying coefficients. *J. Fluid Mech.* **60**, 813–825.

JOHNSON, R. S. 1973*b* On the development of a solitary wave moving over an uneven bottom. *Proc. Camb. Phil. Soc.* **73**, 183–203.

KAKUTANI, T. 1971 Effects of an uneven bottom on gravity waves. *J. Phys. Soc. Japan* **30**, 272.

KARPMAN, V. I. & MASLOV, E. M. 1979 A perturbation theory for the Korteweg–de Vries equation. *Phys. Lett.* **60A**, 307–308.

KAUP, D. J. & NEWELL, A. C. 1978 Solitons as particles and oscillators and in slowly varying media: a singular perturbation theory. *Proc. R. Soc. Lond.* A **361**, 413–446.

KNICKERBOCKER, C. J. & NEWELL, A. C. 1980 Shelves and the Korteweg–de Vries equation. *J. Fluid Mech.* **98**, 803–818.

KNICKERBOCKER, C. J. 1984 Ph.D. Dissertation, Clarkson University.

KORTEWEG, D. J. & DE VRIES, G. 1895 On the change of form of long waves advances in a rectangular canal, and on the new type of long stationary waves. *Phil. Mag.* **39**, 422–443.

LEIBOVICH, S. & RANDALL, J. D. 1973 Amplification and decay of long nonlinear waves. *J. Fluid Mech.* **58**, 481–493.

MILES, J. W. 1979 On the Korteweg–de Vries equation for a gradually varying channel. *J. Fluid Mech.* **91**, pp. 181–190.

NEWELL, A. C. 1978 Soliton perturbation and nonlinear focussing. In *Proc. Symp. on Nonlinear Structure and Dynamics in Condensed Matter. Solid State Physics*, vol. 8, pp. 52–68, Oxford University Press.